Supplementary Information for

Nitric oxide emissions from lakes in the Northern Hemisphere

Wanshan Tan[1], Jintai Lin[1,2,3*], Hao Kong[1], Mengying Wang[1], Sijie Wang[1], Yuhang Zhang[1], Lei Bai[4], Thomas Danckaert[5], Michel Van Roozendael[5], Yong Liu[6], Dianming Wu[7], Lian Feng[8], Xinming Wang[9], Xuejun Liu[10], Guiqian Tang[11], Kun Shi[12], Yunhua Chang[13], and Yujing Mu[14]

[1]Laboratory for Climate and Ocean-Atmosphere Studies, Department of Atmospheric and Oceanic Sciences, School of Physics, Peking University, Beijing, China

[2]Institute of Tibetan Plateau, Peking University, Beijing, China

[3]Institute of Carbon Neutrality, Peking University, Beijing, China

[4]Shanghai Artificial Intelligence Laboratory, Shanghai, China

[5] Royal Belgian Institute for Space Aeronomy (BIRA-IASB), Brussels, Belgium

[6]College of Environmental Sciences and Engineering, State Environmental Protection Key Laboratory of All Material Fluxes in River Ecosystems, Peking University, Beijing, China

[7]Key Laboratory of Geographic Information Science of the Ministry of Education, School of Geographic Sciences, East China Normal University, Shanghai, China

[8]State Key Laboratory of Information Engineering in Surveying, Mapping and Remote Sensing, Wuhan University, Wuhan, China

[9]State Key Laboratory of Advanced Environmental Technology and Guangdong Key Laboratory of Environmental Protection and Resources Utilization, Guangzhou Institute of Geochemistry, Chinese Academy of Sciences, Guangzhou, China

[10]State Key Laboratory of Nutrient Use and Management, College of Resources and Environmental Sciences, China Agricultural University, Beijing, China

[11]State Key Laboratory of Atmospheric Environment and Extreme Meteorology, Institute of Atmospheric Physics, Chinese Academy of Sciences, Beijing, China

[12]Key Laboratory of Lake and Watershed Science for Water Security, Nanjing Institute of Geography and Limnology, Chinese Academy of Sciences, Nanjing, China

[13]State Key Laboratory of Climate System Prediction and Risk Management, Nanjing University of Information Science and Technology, Nanjing, China

[14]Research Center for Eco-Environmental Sciences, Chinese Academy of Sciences, Beijing, China

*Correspondence to Jintai Lin (linjt@pku.edu.cn)

This file includes 22 pages, 16 figures and 4 tables.

Figures

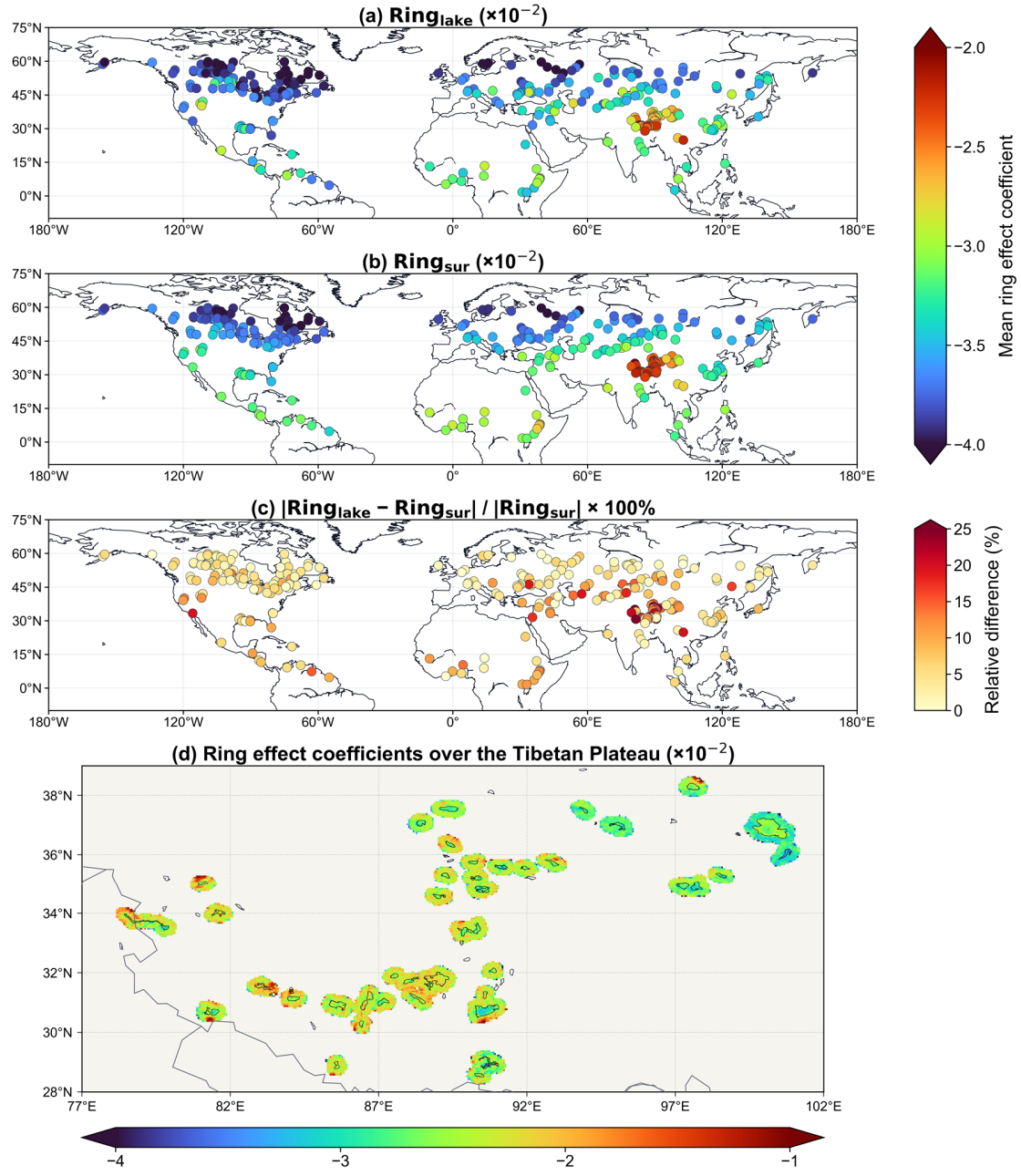


Figure S1. Spatial distribution of fitted Ring effect coefficients from the full-window retrieval. **(a, b)** Ring effect coefficients for each lake ($Ring_{lake}$, averaged from grid cells with the areal proportion of lake water exceeding 90%) and its surrounding ($Ring_{sur}$, averaged within 4 non-lake grid cells of the lake periphery); **(c)** Relative lake–land difference in Ring effect coefficient ($\frac{|Ring_{lake}-Ring_{sur}|}{|Ring_{sur}|} \times 100\ \%$); **(d)** Ring effect coefficients for individual grid cells over the Tibetan Plateau lakes and their surroundings. Only pixels with QA ≥ 0.75 and without sun glint warning are included. Note that the Ring effect is represented as a pseudo-absorption term to account for solar Fraunhofer lines, with the fitted coefficient values in **(a, b, d)** predominantly negative under the adopted sign convention of the pseudo-absorption term.

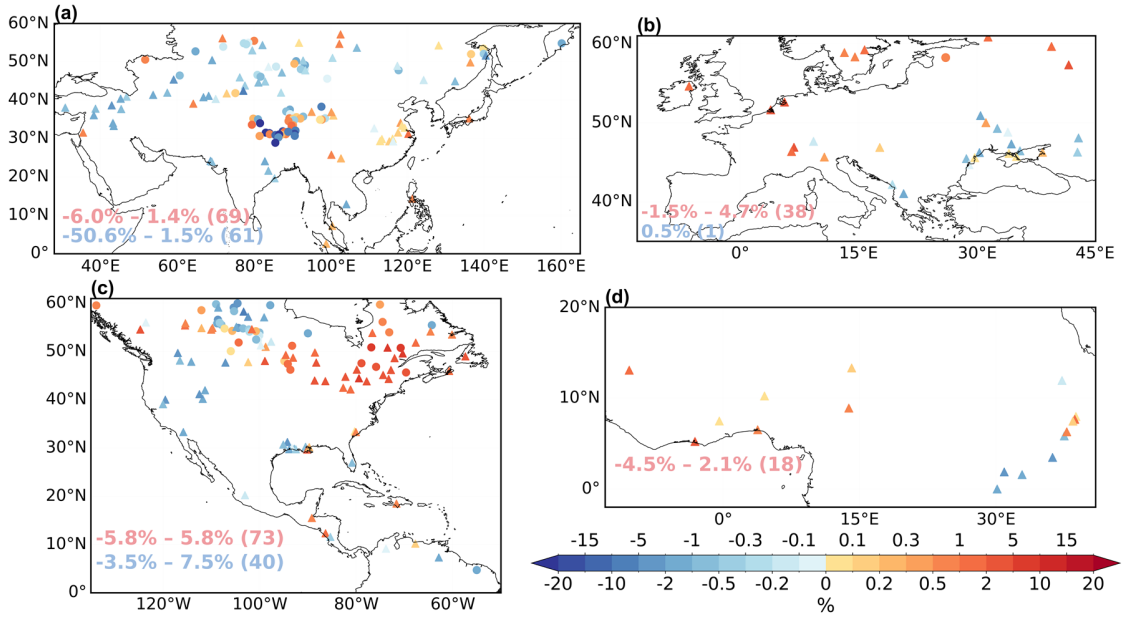


Figure S2. Impact of Screening 2 and 3 on lake NO_2 VCDs. The relative changes of summer average NO_2 VCDs over 2018–2024 after applying Screening 2 and 3. Filled circles and triangles represent natural lakes and human-influenced lakes, respectively. The blue and red numbers in the lower left corner of each panel represent the data range for natural lakes and human-influenced lakes, respectively, and the numbers in parentheses represent the number of lakes.

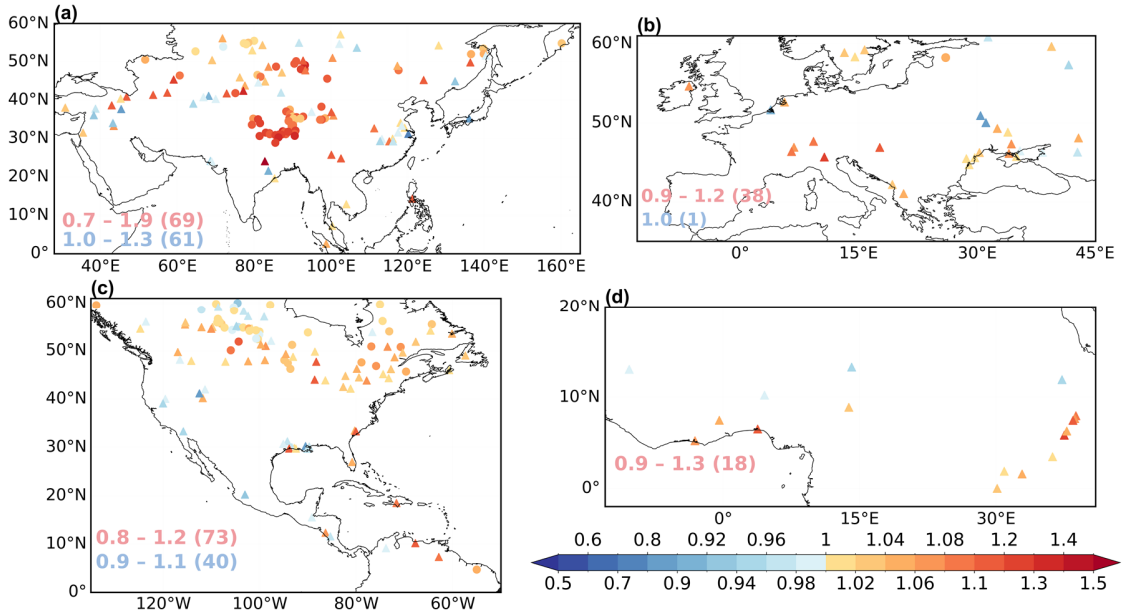


Figure S3. The ratio of lake NO_2 VCDs to their surroundings. The ratio of summer average lake NO_2 VCDs over 2018–2024 to their surroundings. Filled circles and triangles represent natural lakes and human-influenced lakes, respectively. The blue and red numbers in the lower left corner of each panel represent the data range for natural lakes and human-influenced lakes, respectively, and the numbers in parentheses represent the number of lakes.

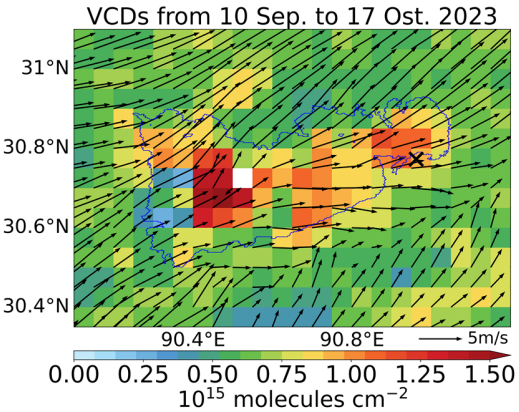


Figure S4. Spatial distribution of average NO_2 VCDs during 10 September to 17 October 2023 over Lake Nam Co. Arrows represent 10 m wind vectors, and the cross marks the location of the in situ site. NO_2 VCDs data after Screening 1–3 are shown. Wind data are taken from the ECMWF analysis.

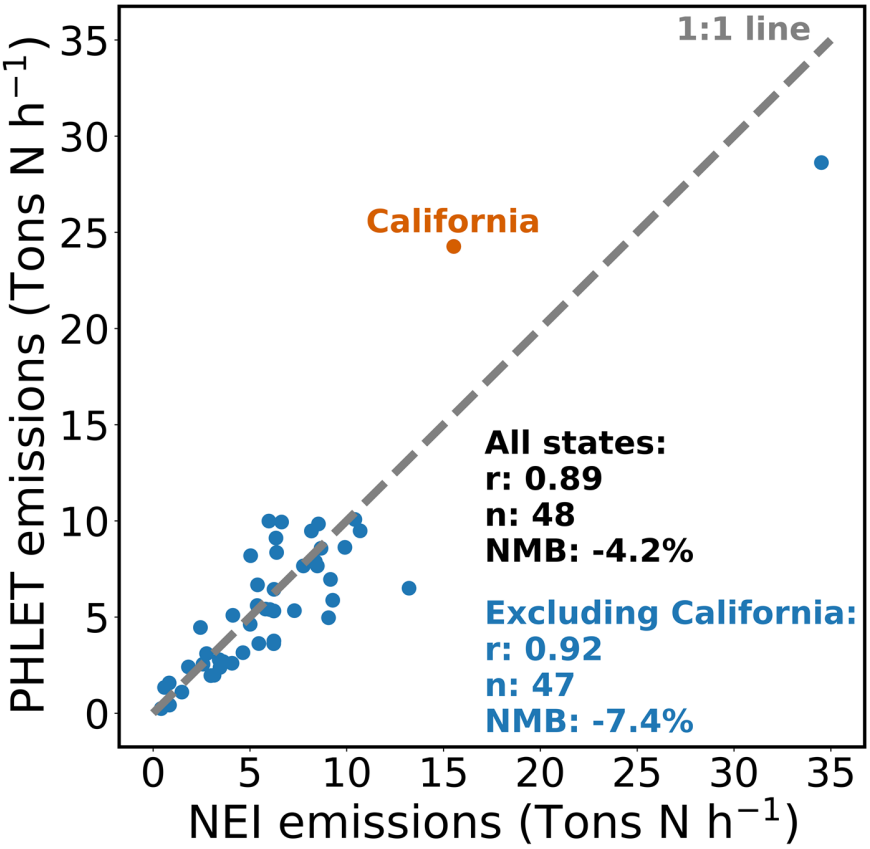


Figure S5. Comparison of anthropogenic NO emissions between NEI and PHLET at the state level. Average summer early afternoon (13:00–14:00 LST) emissions in 2022 are used here. The statistics are presented for the case including (black) and excluding (blue) California.

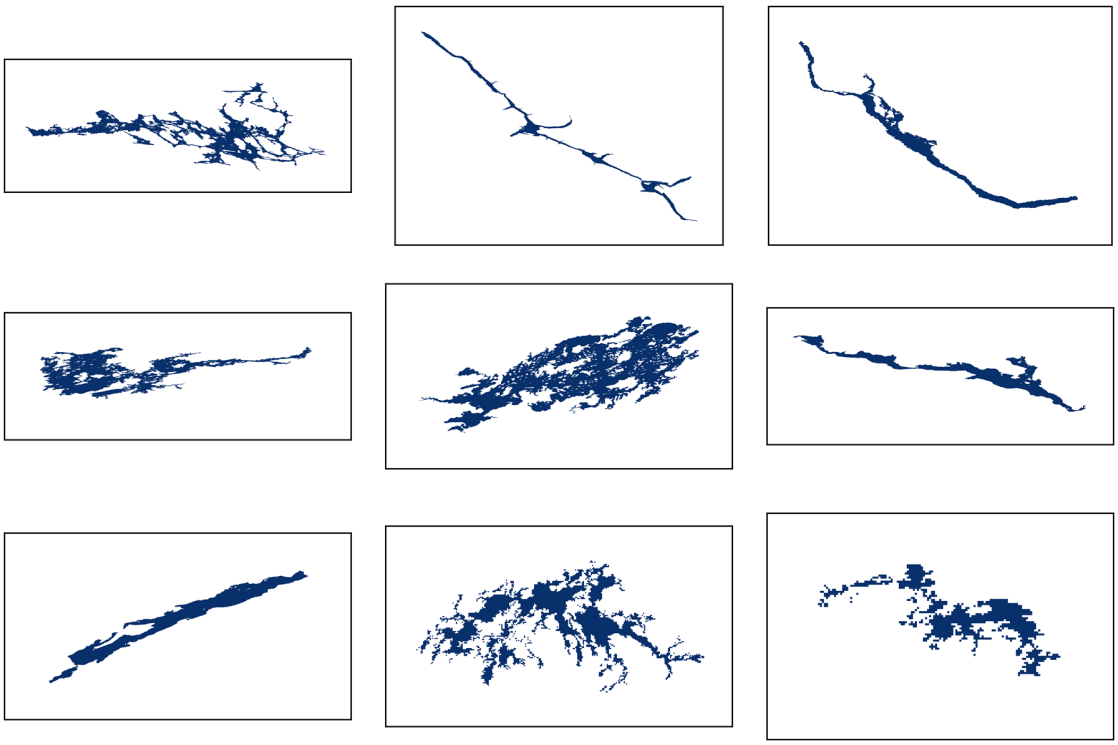


Figure S6. Shapes of nine irregular lakes.

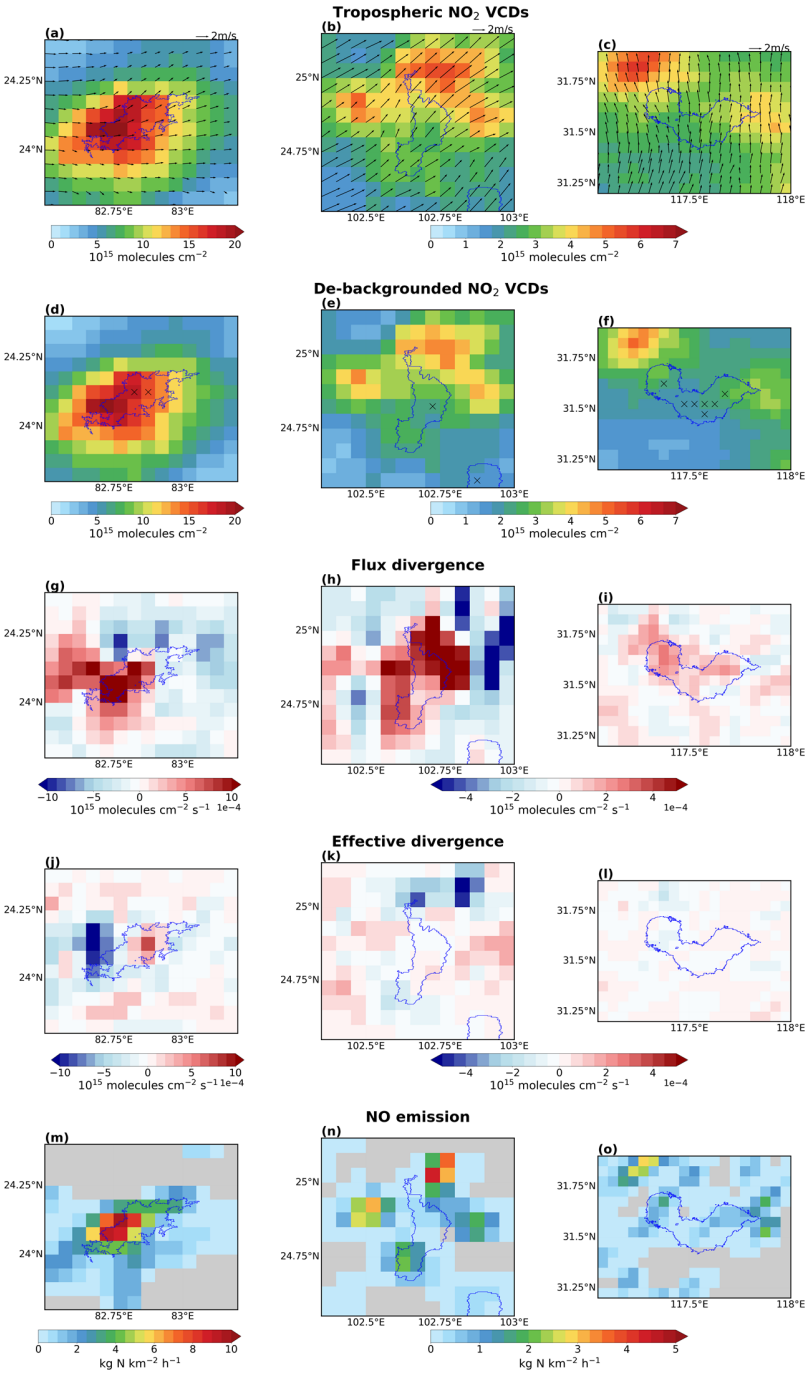


Figure S7. Spatial patterns of NO_2 VCDs, flux divergence terms, effective diffusion terms and NO emissions over three human-influenced lakes with the highest emission intensity and their surroundings in summer 2020. From left to right, the lakes are Govind Ballabah Pant, Dian Chi, and Chao, respectively. **(a–c)** Tropospheric NO_2 VCDs, with superimposed arrows representing the mean wind vectors averaged within 0–500 m above the ground. **(d–f)** De-backgrounded NO_2 VCDs (C); with the black crosses indicating lake-interior grid cells. **(g–i)** Flux divergence terms ($\nabla \cdot (\boldsymbol{VC})$). **(j–l)** Effective diffusion terms ($\nabla \cdot (\boldsymbol{\alpha K} \cdot \nabla \boldsymbol{C})$). **(m–o)** PHLET-derived NO emissions. See previous work (Kong et al., 2022) for the governing equation to connect de-backgrounded NO_2 VCDs and NO emissions that incorporates these individual terms.

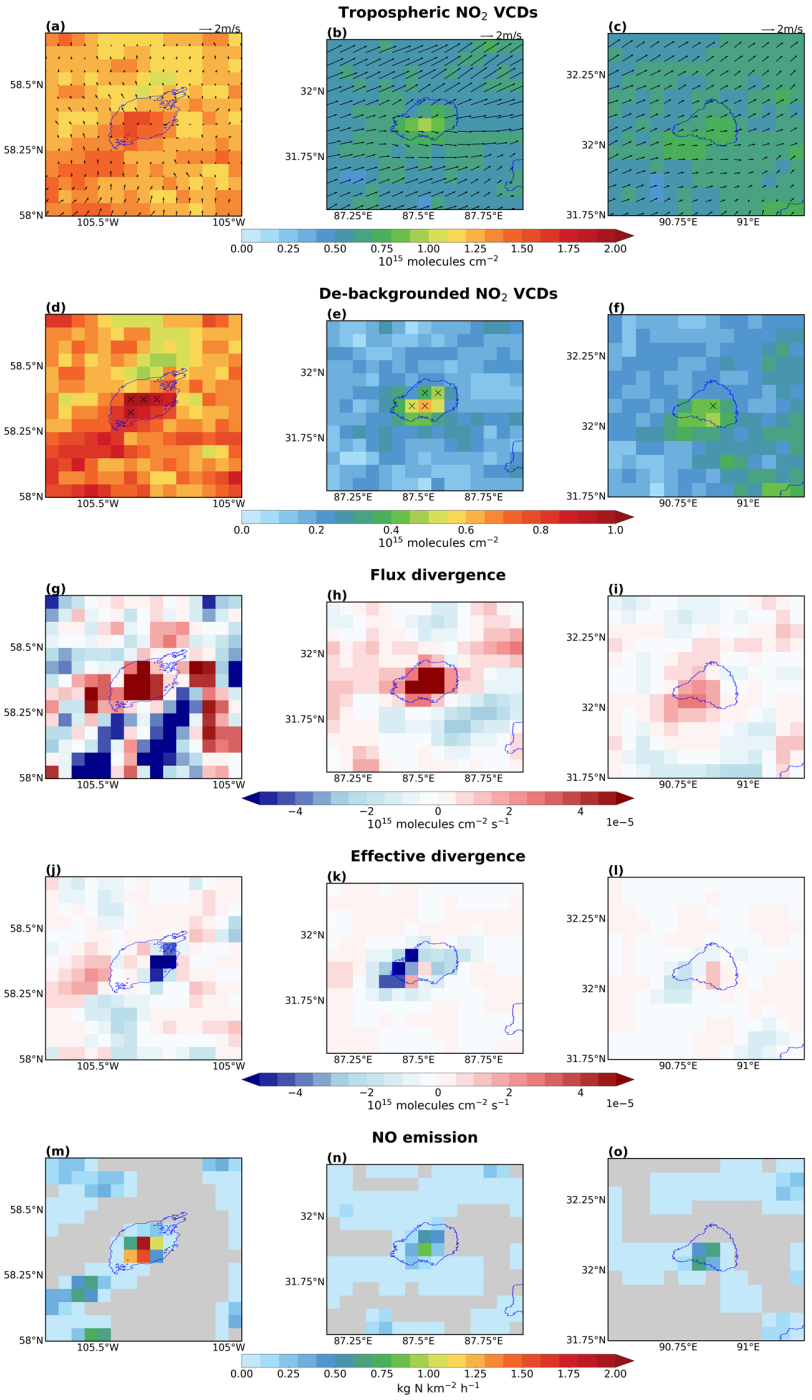


Figure S8. Spatial patterns of NO_2 VCDs, flux divergence terms, effective diffusion terms and NO emissions over three natural lakes with the highest emission intensity and their surroundings in summer 2020. From left to right, the lakes are Pasfield, Ta-tse, and Namru, respectively. **(a–c)** Tropospheric NO_2 VCDs, with superimposed arrows representing the mean wind vectors averaged within 0–500 m above the ground. **(d–f)** De-backgrounded NO_2 VCDs (C); with the black crosses indicating lake-interior grid cells. **(g–i)** Flux divergence terms ($\boldsymbol{\nabla \cdot (VC)}$). **(j–l)** Effective diffusion terms ($\boldsymbol{\nabla \cdot (\alpha K \cdot \nabla C)}$). **(m–o)** PHLET-derived NO emissions. See previous work (Kong et al., 2022) for the governing equation to connect de-backgrounded NO_2 VCDs and NO emissions that incorporates these individual terms.

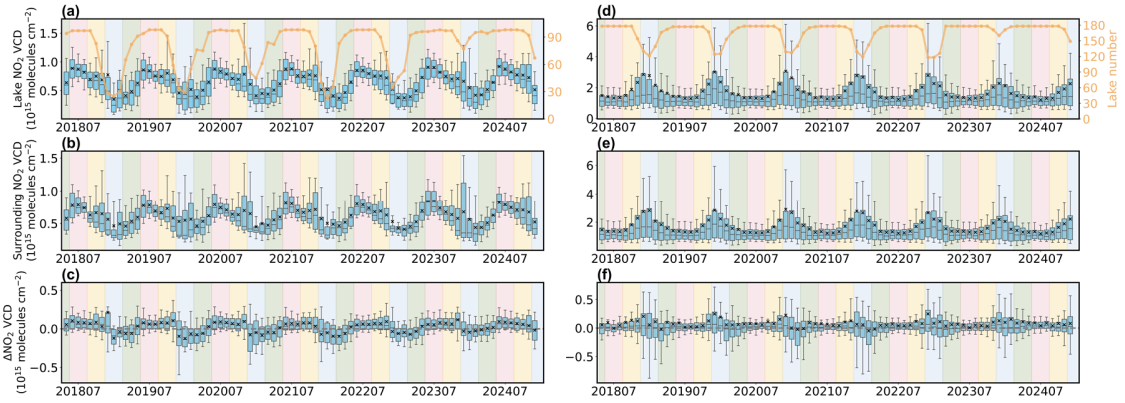


Figure S9. Monthly variation in NO_2 VCDs over lakes and surrounding areas in 2018–2024, with lake NO_2 VCDs calculated using only lake-interior grid cells (Sect. 2.8). **(a, b)** Monthly average NO_2 VCDs over 98 natural lakes and surroundings; **(c)** the difference in NO_2 VCDs between natural lakes and surroundings; **(d, e)** monthly average NO_2 VCDs over 177 human-influenced lakes and surroundings; **(f)** the difference in NO_2 VCDs between human-influenced lakes and surroundings. The yellow lines in **(a)** and **(d)** indicate the number of lakes with valid data. The green, pink, yellow and blue colors in the background denote spring, summer, autumn and winter, respectively. Each box represents the interquartile range (IQR), with the line inside indicating the median value and the cross indicating the mean value. Box whiskers extend to the 10th and 90th percentiles. VCDs data are from the POMINO research product for Asia and the official product for other regions.

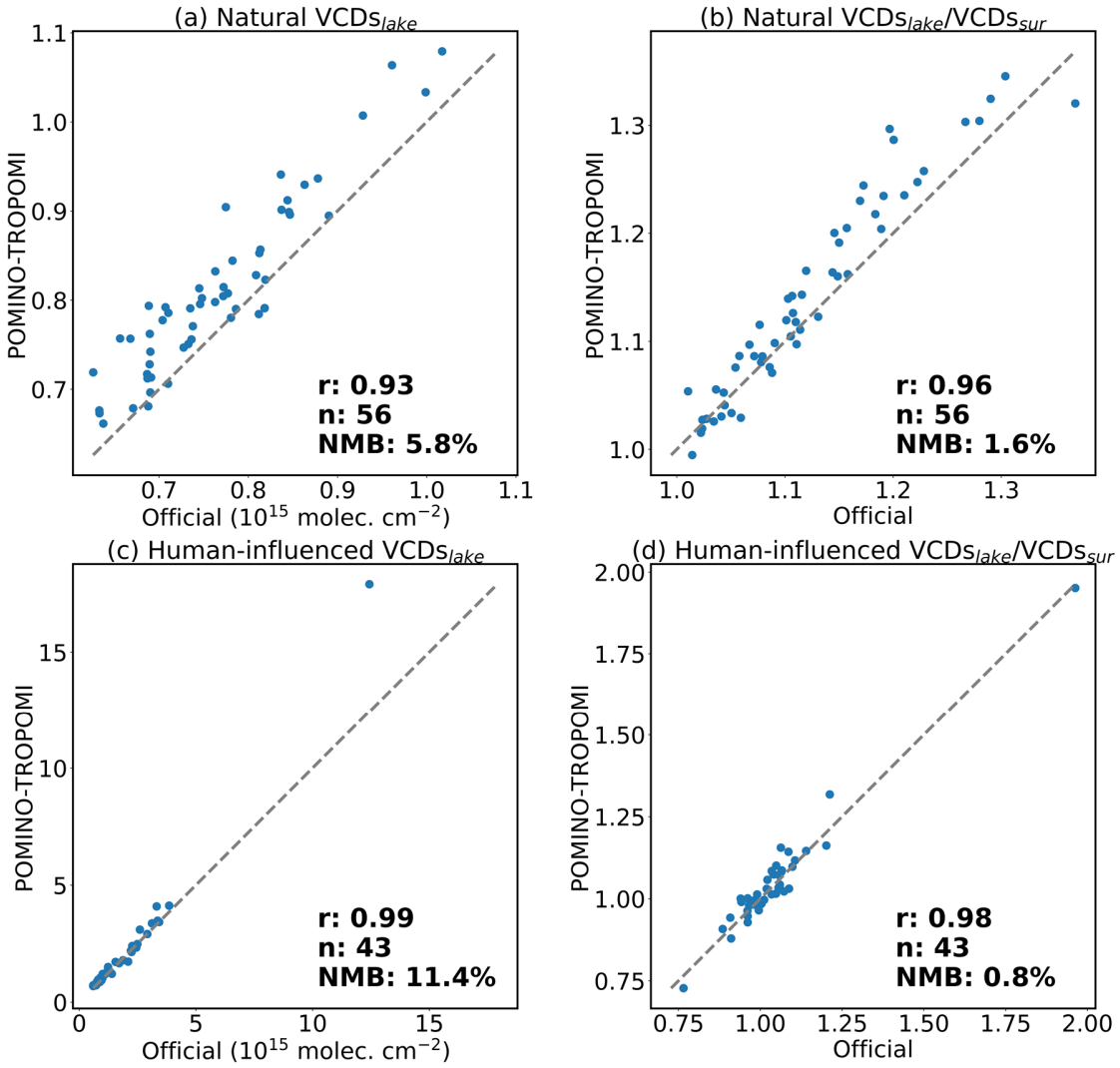


Figure S10. Comparison of POMINO-TROPOMI and official TM5-MP-DOMINO VCD data for lakes in Asia (70°–140° E, 15°–55° N). **(a, c)** Summer-averaged NO_2 VCDs over natural lakes and human-influenced lakes, respectively. **(b, d)** Lake-to-surrounding NO_2 VCD ratios. Note that POMINO-TROPOMI v1.2.2 data used here are available only for Asia.

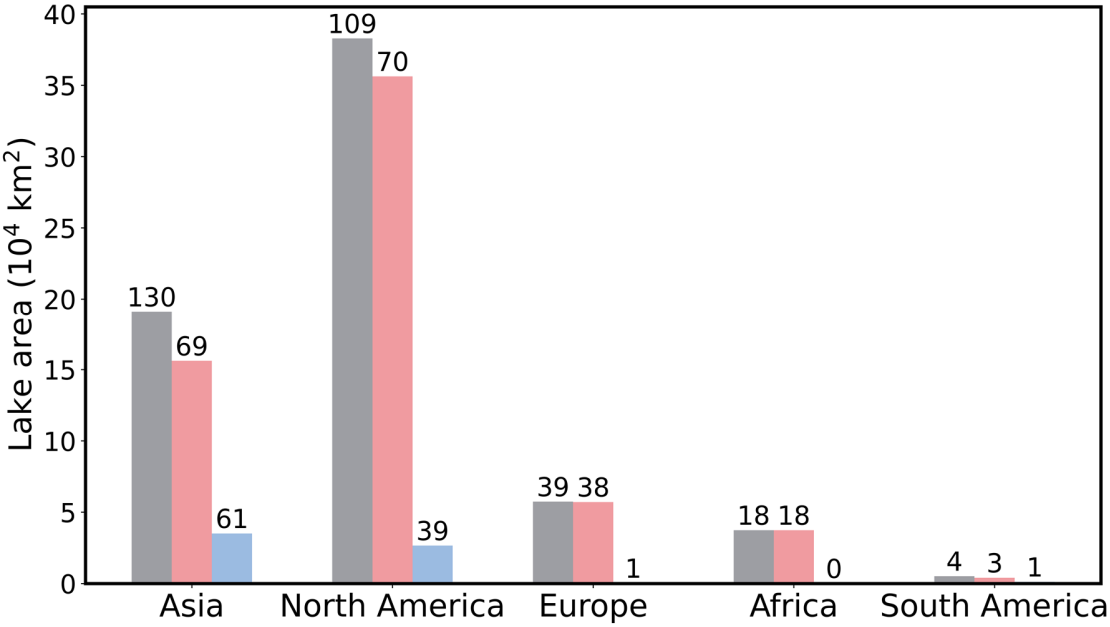


Figure S11. Total lake area in each continent. Red and blue bars are the area of human-influenced lakes and natural lakes, respectively. Grey bars are the total area of all lakes. The numbers at the top of bars denote the number of lakes.

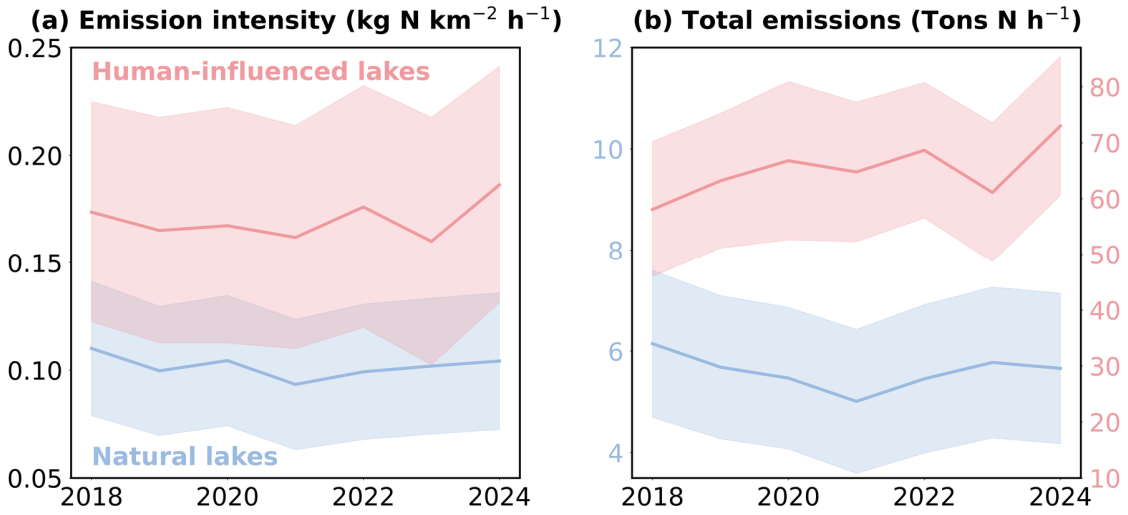


Figure S12. Yearly variation of summertime lake NO emissions. **(a, b)** Yearly variation of average emission intensity and total emissions, respectively. The shaded area represents 1-σ uncertainty. In panel **(b)**, the left and right y-axes represent natural and human-influenced lake emissions, respectively.

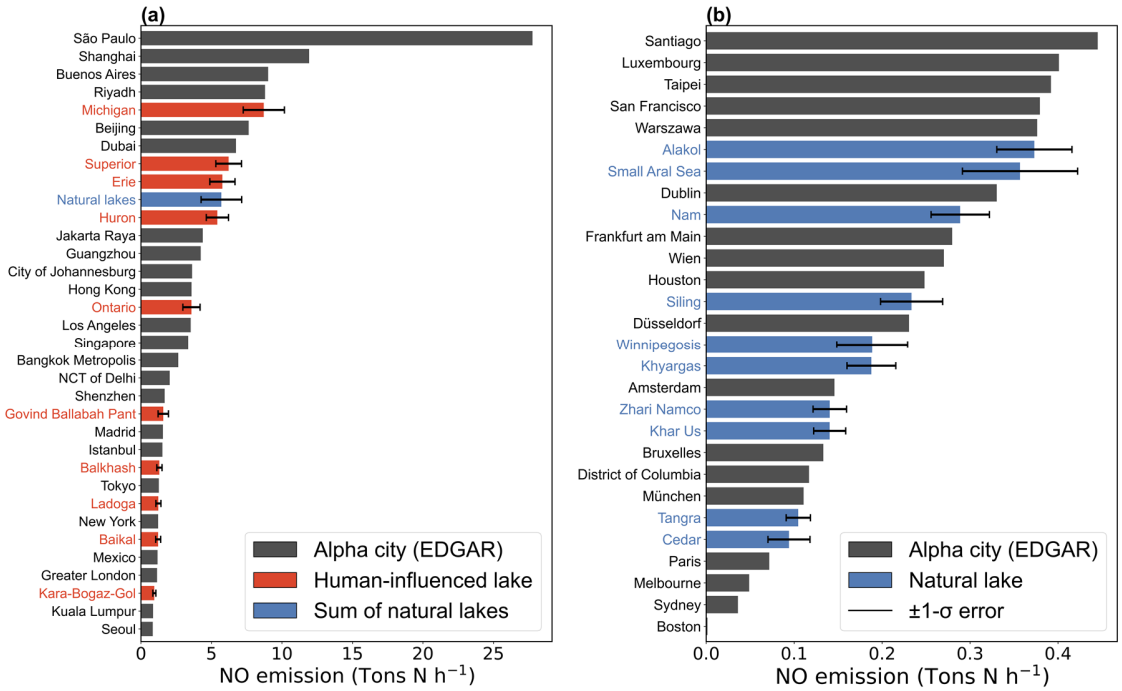


Figure S13. Comparison of NO emissions from lakes and alpha cities (EDGAR v8.1) in summer early afternoon as Fig. 4. Anthropogenic emissions of cities are derived from multi-year average of the EDGAR inventory in 2018–2022.

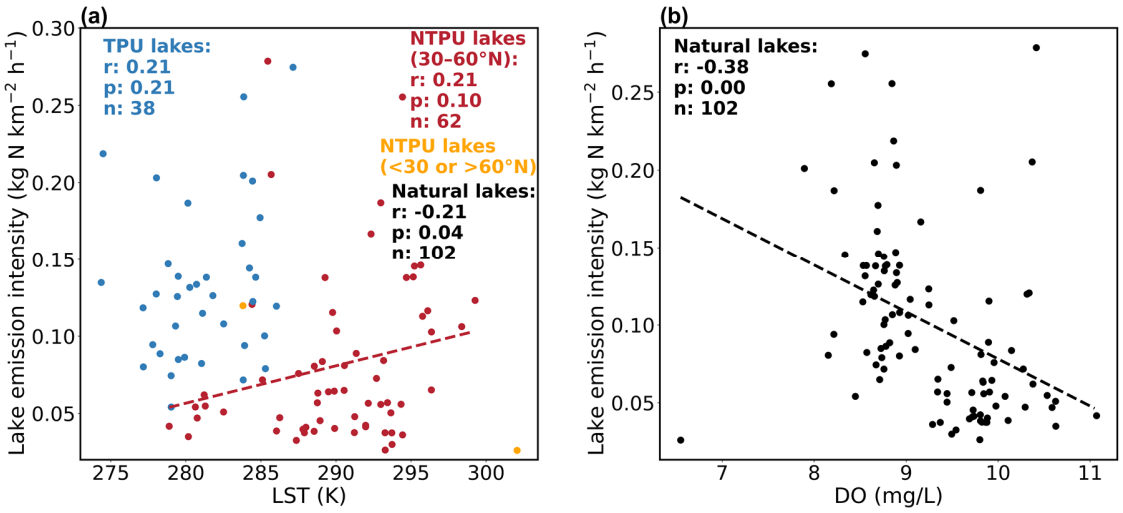


Figure S14. Correlations between NO emission intensity and two environmental factors for natural lakes. **(a)** Scatter plot for NO emission intensity and LST. Red dots with respective statistics are for mid-latitude non-Tibetan-Plateau (NTPU) lakes, and blue dots are for Tibetan-Plateau (TPU) lakes. Black numbers represent the statistics for all natural lakes. **(b)** Scatter plot for NO emission intensity and DO for all natural lakes.

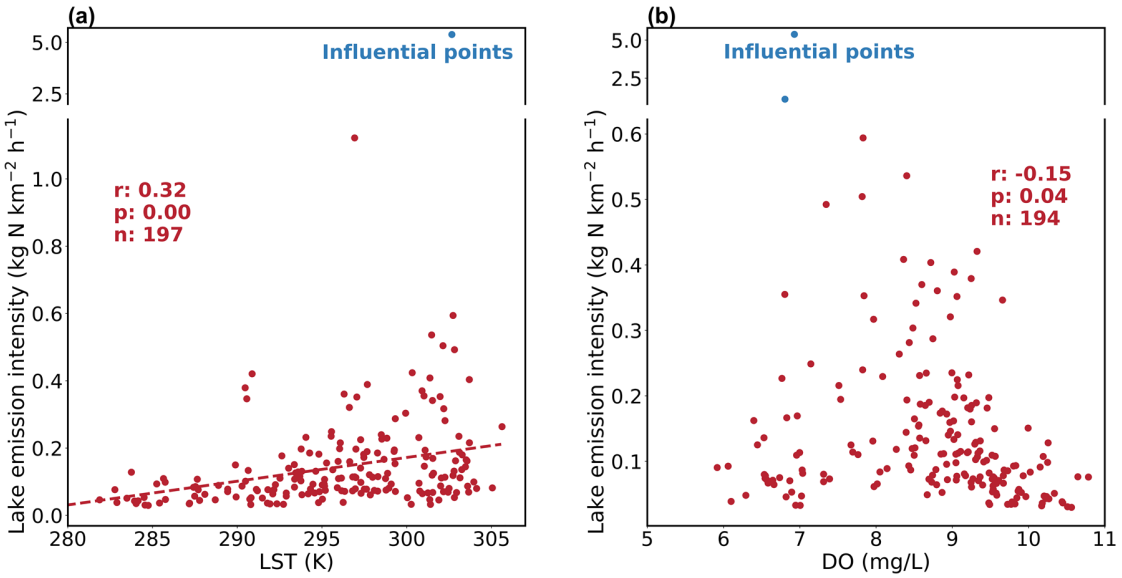


Figure S15. Correlations between emission intensity and two environmental factors for human-influenced lakes. Blue dots represent influential (i.e., outlier) data points identified by the Cooks distance with the empirical threshold of 4/n (n=198); these points are not included in the statistics to prevent the regression results from being dominated by a small number of points.

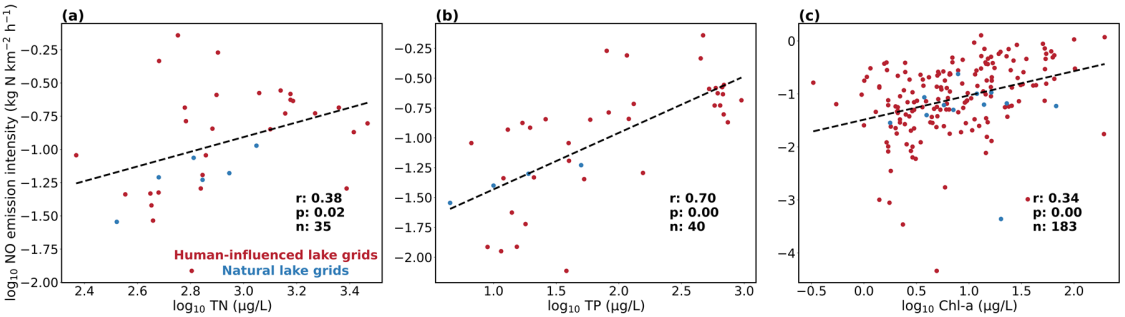


Figure S16. Correlations between emission intensity and three in situ environmental factors at grid-cell scale. Red dots denote grid cells in human-influenced lakes, and blue dots denote grid cells in natural lakes. Black numbers represent the statistics based on all data, and black dashed line represents the linear fitted curve for all data.

Tables

Table S1. Impact of Screening 2 and 3 on lake NO_2 VCDs. The relative change in summer average NO_2 VCDs from 2018 to 2024 over eight TP lakes after removing pixels with negative H_2O SCDs or sun glint, as well as the lake-to-surrounding ratio in NO_2 VCDs. These eight lakes are most affected by Screening 2 and 3.

Lake name	Relative change (decrease by more than 10%)	Lake-to-surrounding ratio
Ngangla Ringco	-50.59%	1.27
Tangra	-33.30%	1.21
Lumajangdong	-27.49%	1.23
P'ei-k'u t'so	-26.48%	1.20
Cha-pu-yeh ch'a-k'a	-20.01%	1.30
Pa-Mu-Ts'o	-17.46%	1.16
Ta-tse	-16.30%	1.34
Zhari Namco	-12.46%	1.26

Table S2. The comparison of in situ NO_2 concentrations with satellite observations.

Lake	In situ measurement				Satellite data [1]	
	Method	Time	Measurement location and height	NO_2 observation	Time	NO_2 observation
Ontario (Human-influenced, in North America)	Sailboat-mounted Aeroqual 500 hand-held monitors	LST 14:00–16:00, 15-Jun, 01-Jul, 17-Jul and 29-Jul 2024	Eastern offshore; about 1.5 m over the water	6.1–17.4 ppb (Donaldson, 2026)	Same dates as in situ measurements	1.4–4.0 ppb [2]
Michigan (Human-influenced, in North America)	Aircraft in-situ spiral vertical profiling	LST 14:00–17:00, 02-Jun 2017	[87.65 ° W, 43.75 ° N], [87.65°W,43.1 ° N], and [87.65°W,42.45°N]; surface–3km	2.8–5.3 × 10^{15} molec. cm^{-2} (Stanier et al., 2021)	Jun 2018	1.7–2.4 × 10^{15} molec. cm^{-2} [3]
Taihu (Human-influenced, in Asia)	Shipboard Thermo 42i-TL chemiluminescence analyzer	LST 13:00–14:00 12–13 August 2023	Across the lake; surface	6–8 ppb (unpublished data from the author team)	Same dates as in situ measurements	2.4–2.5 ppb [2]
Nam Co (Natural, in Asia)	Thermo Scientific 42CTL	LST 13:00–14:00,10-Sep to 17-Oct 2023	[90.96 ° E, 30.77 ° N]; surface	2.6 ppb (Kong et al., 2024)	Same dates as in situ measurements	2.0 ppb [2]

[1] Satellite data for North America and Asia are from the official TROPOMI product and POMINO-TROPOMI, respectively.

[2] NO_2 column is converted to surface mixing ratio following previous work (Zhang et al., 2023; Wang et al., 2026).

[3] Tropospheric column, with a slight contribution from the free troposphere above 3 km.

Table S3. NO_2 VCDs over natural lakes and surrounding areas in each season. * means the difference between VCDs over lakes and surroundings is statistically significant (Wilcoxon signed-rank test upon all lakes, $p < 0.01$).

mean ± std (median)	Winter	Spring	Summer *	Autumn *
lakes	0.50 ± 0.42 (0.38)	0.54 ± 0.26 (0.49)	0.83 ± 0.20 (0.81)	0.73 ± 0.31 (0.66)
surroundings	0.53 ± 0.41 (0.39)	0.54 ± 0.24 (0.49)	0.77 ± 0.20 (0.73)	0.66 ± 0.30 (0.58)

Table S4. NO_2 VCDs over human-influenced lakes and surrounding areas in each season.

mean ± std (median)	Winter	Spring	Summer	Autumn
Lakes	2.41 ± 3.26 (1.54)	1.51 ± 2.18 (1.12)	1.35 ± 1.35 (1.11)	1.78 ± 2.26 (1.27)
surroundings	2.29 ± 2.72 (1.55)	1.46 ± 1.56 (1.11)	1.30 ± 0.95 (1.08)	1.70 ± 1.80 (1.25)

Reference:
Donaldson, D. J.: Sailboat Measurements of Trace Gases in Urban Environments: In Toronto, Canada, Ground-Level NO2 Is Consistently Elevated over Lake Ontario versus at the Shoreline, but O3 Is Not, ACS Earth and Space Chemistry, 10, 1543-1553, 10.1021/acsearthspacechem.6c00049, 2026.
Kong, H., Lin, J., Chen, L., Zhang, Y., Yan, Y., Liu, M., Ni, R., Liu, Z., and Weng, H.: Considerable Unaccounted Local Sources of NO_x Emissions in China Revealed from Satellite, Environmental Science & Technology, 56, 7131-7142, 10.1021/acs.est.1c07723, 2022.
Kong, H., Lin, J., Tang, G., Zhang, Y., Li, C., Xu, C., Shen, L., Liu, X., Yang, K., Su, H., Xu, W., and Tan, W.: Reply to: NO_2 satellite retrievals biased by absorption in water, Nature Geoscience, 17, 976-978, 10.1038/s41561-024-01546-7, 2024.
Stanier, C. O., Pierce, R. B., Abdi-Oskouei, M., Adelman, Z. E., Al-Saadi, J., Alwe, H. D., Bertram, T. H., Carmichael, G. R., Christiansen, M. B., Cleary, P. A., Czarnetzki, A. C., Dickens, A. F., Fuoco, M. A., Hughes, D. D., Hupy, J. P., Janz, S. J., Judd, L. M., Kenski, D., Kowalewski, M. G., Long, R. W., Millet, D. B., Novak, G., Roozitalab, B., Shaw, S. L., Stone, E. A., Szykman, J., Valin, L., Vermeuel, M., Wagner, T. J., Whitehill, A. R., and Williams, D. J.: Overview of the Lake Michigan Ozone Study 2017, Bulletin of the American Meteorological Society, 102, E2207-E2225, 10.1175/bams-d-20-0061.1, 2021.
Wang, M., Lin, J., Zhang, Y., Jin, X., Tan, W., Kong, H., and Wang, S.: Satellite Retrieval of Tropospheric NO2 under Fire Conditions, EGUsphere [preprint], 10.5194/egusphere-2026-2410, 2026.
Zhang, Y., Lin, J., Kim, J., Lee, H., Park, J., Hong, H., Van Roozendael, M., Hendrick, F., Wang, T., Wang, P., He, Q., Qin, K., Choi, Y., Kanaya, Y., Xu, J., Xie, P., Tian, X., Zhang, S., Wang, S., Cheng, S., Cheng, X., Ma, J., Wagner, T., Spurr, R., Chen, L., Kong, H., and Liu, M.: A research product for tropospheric NO2 columns from Geostationary Environment Monitoring Spectrometer based on Peking University OMI NO2 algorithm, Atmospheric Measurement Techniques, 16, 4643-4665, 10.5194/amt-16-4643-2023, 2023.